Frustration-controlled quantum phase transition between multiple singular two-stage Kondo behaviors in a tetrahedral quadruple quantum dot structure

Peng-Chao Wang,[1] Yi-Hui Wang,[1] Chong Chen,[1] Jun Zhang,[1] Wei Li,[1] Nan Nan,[1,2] Jia-Ning Wang,[1] Jun-Tao Yang,[1] Amel Laref,[1,3] and Yong-Chen Xiong[1,4,*]

[1]*School of Mathematics, Physics and Optoelectronic Engineering, and Collaborative Innovation Center for Optoelectronic Technology, Hubei University of Automotive Technology, Shiyan 442002, People's Republic of China*

[2]*State Key Laboratory of Advanced Technology for Materials Synthesis and Processing, Wuhan University of Technology, Wuhan 430070, People's Republic of China*

[3]*Department of Physics and Astronomy, Science Faculty, King Saud University, Riyadh 11451, Saudi Arabia*

[4]*Shiyan Bureau of Science and Technology, 16 Chaoyang North Road, Shiyan 442000, People's Republic of China*

(Received 5 November 2021; revised 24 January 2022; accepted 15 February 2022; published 25 February 2022)

Semiconductor quantum dots are considered to be promising candidates for the hardware of quantum information technology and optoelectronic devices. Herein, motivated by a tetrahedrally shaped colloidal quadruple quantum dot structure made from In-based III–V semiconductors, which has been synthesized very recently by Leemans *et al.* [J. Am. Chem. Soc., **143**, 4290 (2021)], we provide timely insight into the electronic transport and the quantum phase transition (QPT) for such an architecture. When the interdot hopping between different side dots (t_2) is absent, a singular two-stage Kondo effect is revealed for small central-side coupling t_1. The two screening processes are separated by an energy scale of the Ruderman-Kittel-Kasuya-Yosida (RKKY) interaction, and the fitting parameters deviate from the regular ones of the side-coupled double dot system. The RKKY interaction and temperature are well illustrated by functions of $t_1^4/(UT_{K1}^2)$, where U and T_{K1} are the on-site electron-electron repulsion and the first Kondo temperature, respectively. When t_2 turns on, the ground state of the side dots transits from a spin quadruplet to a magnetic frustration phase, and then to a singlet, through two first-order QPTs. In the frustration phase, another new two-stage Kondo effect is demonstrated, which includes the process of screening the local spin on the central dot firstly, and then that on the neighborless side dot is screened at a lower temperature. Both the Kondo temperatures are found to be rather sensitive to t_2. When t_2 is large enough, the reappearance of the regular Kondo effect is found. With fixed $t_2 = 0$, charging the central dot triggers a transition from an antiferromagnetic correlation among the side dots to a ferromagnetic one, accompanied by a Kondo behavior in the central dot. We adopt the state-of-the-art numerical renormalization group method to implement the above behaviors, combined with analytical arguments.

DOI: 10.1103/PhysRevB.105.075430

I. INTRODUCTION

Quantum information technology (QIT) has made remarkable progress during the last two decades, moving from Nobel Prize winning experiments to a multidisciplinary field that spans from basic algorithms to industrial-scale developments. The basic unit of a QIT device is the quantum bit, or qubit, which can perform some exact computational operations using two well-defined quantum states, i.e., $|0\rangle$ and $|1\rangle$. Currently, several physical platforms have been proposed as the potential hardware of qubits, including defects and impurities in solids [1–3], photons [4], trapped ions [5,6], superconducting circuits [7,8], magnetic and nonmagnetic molecules [9–12], and semiconductor quantum dots (QDs) [13,14]. Semiconductor qubits are in this list, primarily due to their potential for high-density integration on a large scale, long coherence times, fast two-qubit gates, and fault-tolerant operations [15].

Implementation of QD-based qubits typically makes use of a pair of electron reservoirs (leads). These reservoirs play vital roles during the initial setup of the device to the required few-electron regime [16]. Also, based on such designs, one could deal with the charge or spin transport property of the QD structures, which also attracts much attention. On the other hand, interactions between QDs and their environments—although they may result in unwanted consequences, such as decoherence in qubits [17]—can also be exploited as ideal platforms for the discoveries of some novel physical phenomena which are difficult to obtain in bulk materials, such as the Kondo effect [18–21], quantum interference [22,23], the Coulomb blockade effect [24–26], the QPT [27–31], the Fano effect [32,33], Fermi-liquid and non-Fermi-liquid behaviors [34–36], and so on. Generally speaking, these behaviors depend closely on the QD and electrode materials, the number and configurations of the QDs, and the interactions which are taken into account.

Tremendous progress having been made in understanding the above phenomena for single, double, and triple quantum dot structures, research interest has now turned to quadruple

*xiongyc_lx@huat.edu.cn

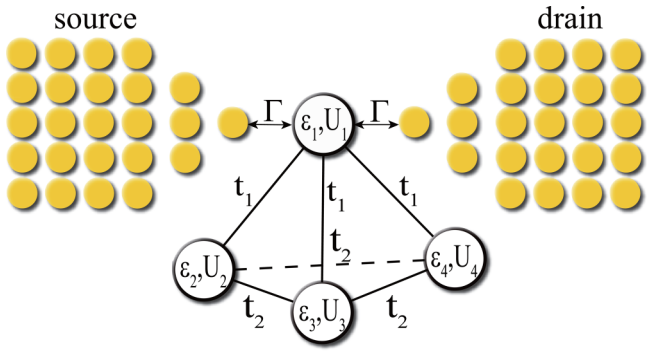

FIG. 1. Schematic illustration of the tetrahedral quadruple quantum dot connected to the source (S) and drain (D) electrodes. Dot 1 (the central dot) connect directly to the electrodes, whereas the side dots (dots 2, 3, and 4) have no direct connection to the electrodes. t_1 illustrates the interdot hopping integral (tunneling coupling) between the central and the side dots, and t_2 is that between different side dots.

QD (QQD) systems in terms of both experimental and theoretical aspects. For instance, in a QQD structure with one continuous channel and two concrete channels, Jiang and Han studied the quantum coherent transport in both the absence and presence of a magnetic field [37]. For a QQD system with a squarelike configuration, Liu *et al.* revealed the competition among the Heisenberg, Kondo, and Ising types of interactions [38]. In a QQD setup including two double quantum dots (DQDs) coupled to superconducting electrodes, Sothmann *et al.* studied the possibility of generating a fractional Josephson effect [39]. In a QQD device containing two coupled DQDs, a Kondo effect switcher was demonstrated when both the intra- and inter-DQD couplings were considered simultaneously [40]. For a QQD cell, Kagan *et al.* predicted that the presence of the insulating bands might result in the emergence of spin-polarized windows in an external magnetic field [41]. For a QQD ring with moderate Coulomb interaction, the local magnetic moment formation and electronic transport were described at and away from equilibrium [42]. For a QQD in spinless and spinful regimes, the charge Kondo effect was demonstrated by using the scattering T-matrix method, Fermi-liquid theory, and poor man's scaling [43]. Furthermore, for the purpose of practical applications, various technological approaches were suggested to scale up the number of qubits [44–46], to coherently manipulate electrons [16,47] and their spins [48,49], and to measure the internal interactions [50,51] based on various QQD structures.

Very recently, Leemans *et al.* reported a tetrahedrally shaped colloidal QQD structure made from In-based III–V semiconductors [52]. Motivated by this fascinating architecture, here we provide a timely study of the charge transport, the thermodynamical properties, and the QPT of such a system in the strongly correlated limit. We consider a typical case where only one dot (the central dot) connects directly to two electrodes whereas the other dots (the side dots) do not have a direct connection to the electrodes. A schematic illustration is presented in Fig. 1. We find a singular two-stage Kondo effect, if the interdot hopping integral between different side dots (t_2) is absent and $J_1 \ll T_{K1}$. Here, J_1 is the effective exchange coupling between the central dot and the side dots, and T_{K1} is the Kondo temperature of the model without side dots. The first screening stage at T_{K1} belongs to the regular Kondo effect, whereas the second one at T_{K2} results from J_1. Interestingly, they are separated by an energy scale T_{RKKY} due to the ferromagnetic RKKY interaction J_{RKKY} between different side dots mediated by J_1. Around T_{RKKY}, the tetrahedral QQD (TQQD) locks into a high-spin state, and two sharp peaks develop in the local density of states (LDOS) of the side dot. Full conductance only exists in the regime $T_{K2} < T \leqslant T_{K1}$. We conclude that T_{K2} could be illustrated by an exponential function of T_{K1}, but the orders of the fitting parameters are quite different from those in the side-coupled DQD (SDQD) structures. A relation between J_{RKKY} (T_{RKKY}) and t_1 is also revealed, which is consistent with our numerical results. Here, t_1 is the hopping between the central and the side dots. When t_2 sweeps upwards, the ground state of the side dots at zero temperature transits from a spin quadruplet to a magnetic frustration phase, and then to a singlet, through two first-order QPTs. In the frustration phase, the quantum state of the TQQD is dominated by a state where electrons on two of the side dots generate a singlet whereas the electron on the remaining side dot forms another singlet with that on the central dot. This electron configuration provides us an ideal platform for the discovery of the QPT between two singular two-stage Kondo effects if the fixed $t_1 \sim T_{K1}$. In this case, this new two-stage Kondo effect includes the process where the local spin on the central dot is screened by the electrodes firstly, and then that on the remaining side dot is screened by t_1. One also finds that in this Kondo behavior, T_{K1} and T_{K2} are rather sensitive to t_2. For t_2 in the third quantum phase, the total charge number of the side dots drops to 2.0, and these dots form a spin singlet due to t_2 and decouple from the central dot; hence the reappearance of the ordinary Kondo effect could be found. For $t_1 \gg T_{K1}$, the Kondo effect is partially recovered around T_{K1}, and the competition between the direct and indirect exchange interactions is clearly revealed by the LDOS of the side dots. When the energy level of the central dot sweeps downwards, one finds QPTs from an antiferromagnetic correlation among the side dots to a ferromagnetic one, and then to an antiferromagnetic one, associated with Kondo resonances in the LDOS of the central dot.

It is noticed that the TQQD structure is a typical system which may exhibit magnetic frustration [53]. It may also appear as a building block of quantum network devices [54,55]. Furthermore, owing to the complex geometry and many more Feynman paths for electron transmission, the TQQD may possess a rather rich phase diagram, making it promising for the development of multifunctional QIT devices [56], as well as a prototype for studying the competition among different many-body phenomena, such as the Kondo effect, RKKY interaction, magnetic frustration, and the QPT, which are our focus points in the following discussion.

II. MODEL AND METHOD

The second quantized Hamiltonian of the TQQD system is written as a four-impurity Anderson model, where dot 1 (the central dot) is connected directly to the source (S) and drain (D) electrodes, whereas the other dots (the side dots, labeled as dots 2, 3, and 4, respectively) have no direct connections to

the conduction leads:

$$H = H_\gamma + H_{\rm TQQD} + H_{\rm hyb}, \tag{1}$$

with

$$H_\gamma = \sum_{\gamma k\sigma} \epsilon_{\gamma k\sigma} c^\dagger_{\gamma k\sigma} c_{\gamma k\sigma}, \tag{2}$$

$$\begin{aligned} H_{\rm TQQD} = & \sum_{i=1}^{4} \left(\sum_\sigma \epsilon_i n_{i\sigma} + U_i n_{i\uparrow} n_{i\downarrow} \right) \\ & - t_1 \sum_{i=2}^{4} \sum_\sigma (d^\dagger_{1\sigma} d_{i\sigma} + {\rm H.c.}) \\ & - t_2 \sum_\sigma (d^\dagger_{2\sigma} d_{3\sigma} + d^\dagger_{3\sigma} d_{4\sigma} + d^\dagger_{4\sigma} d_{2\sigma} + {\rm H.c.}), \end{aligned} \tag{3}$$

$$H_{\rm hyb} = \sum_{\gamma k\sigma} \tau_{\gamma k} (c^\dagger_{\gamma k\sigma} d_{1\sigma} + {\rm H.c.}). \tag{4}$$

Here, $H_\gamma (\gamma = S, D)$ represents the contribution of the noninteracting metal electrode. $\epsilon_{\gamma k\sigma}$ is the single-electron energy in electrode γ, $c^\dagger_{\gamma k\sigma}$ ($c_{\gamma k\sigma}$) is the creation (annihilation) operator for conduction electrons with wave vector k and spin σ ($\sigma = \uparrow$ or $\downarrow$). $H_{\rm TQQD}$ is the Hamiltonian of the TQQD. $n_{i\sigma} = d^\dagger_{i\sigma} d_{i\sigma}$ is the number operator for spin-σ electrons in dot i; $n_i = n_{i\uparrow} + n_{i\downarrow}$. ϵ_i and U_i are the single-electron energy and the electron-electron Coulomb interaction, respectively. t_1 illustrates the interdot hopping integral (tunneling coupling) between the central dot and the side dots, and t_2 is that between different side dots. Finally, $H_{\rm hyb}$ is the contribution of the hybridization between the conduction band and dot 1; $\tau_{\gamma k}$ is the tunneling coupling, which is assumed to be source-drain symmetric and k, σ independent, and hence we omit its subscript in the following.

In this paper, we mainly focus on the QPT and electronic transport in the strongly correlated limit. In such a situation, schemes based on standard density functional theory (DFT) for simulations of strongly correlated behaviors such as the Kondo effect remain challenges to date. Therefore we adopt Wilson's numerical renormalization group (NRG) method [57–59] to solve Eq. (1). The NRG is a nonperturbative technique for treating low-temperature properties of quantum impurity systems and is regarded as one of the very few computational tools which give reliable information on both the static and dynamic properties for strongly correlated problems. In our NRG performance, we chose the renormalization parameter Λ, which discretizes the conduction bands logarithmically, to be ∼2.5–3.0, and we retain around 3000 low-lying energy states at each iteration. For the sake of simplicity, we take a wide flat conduction electron density of states (DOS) $\rho_0 = 1/(2W_b)$, which is the generic case relevant to most metallic bands, where W_b is the half bandwidth. Therefore the hybridization function $\Gamma = \pi \rho_0 \tau^2$ is defined inside the band and becomes a constant.

III. EFFECTIVE MODEL AND PHYSICAL QUANTITIES

Since the most fascinating physical behavior arises when the TQQD is in essence half filled, we mainly consider the representative case where ϵ_i satisfies particle-hole (p-h) symmetry, $\epsilon_i = -U_i/2$, except in Sec. IV D. In such a situation, and if $t_1, t_2, \tau \ll U$, by performing a Schrieffer-Wolff transformation [60] up to the second-order perturbation on the tunnel-coupling terms, one obtains an effective Hamiltonian as follows:

$$H_{\rm eff} = H_\gamma + J_0 \hat{S}_1 \cdot \hat{s}_0 + \sum_{i=2}^{4} J_1 \hat{S}_1 \cdot \hat{S}_i + \sum_{i,j=2, i<j}^{4} J_2 \hat{S}_i \cdot \hat{S}_j. \tag{5}$$

Here, $\hat{S}_i = \sum_{\sigma\sigma'} d^\dagger_{i\sigma} \frac{\hat{\sigma}_{\sigma\sigma'}}{2} d_{i\sigma}$ ($i \approx 1$–4) is the spin operator of dot i, $\hat{s}_0 = \sum_{\sigma\sigma'} c^\dagger_\sigma \frac{\hat{\sigma}_{\sigma\sigma'}}{2} c_\sigma$ is the electron spin density of the conduction band belonging to the electrodes, and $\hat{\sigma}_{\sigma\sigma'} = (\sigma_x, \sigma_y, \sigma_z)$ is a vector composed by the Pauli matrices. Furthermore,

$$J_0 = 2\tau^2 \left(\frac{1}{|\epsilon_1|} + \frac{1}{|\epsilon_1 + U_1|} \right) \tag{6}$$

is the exchange constant between $\hat{S}_1$ and $\hat{s}_0$, and

$$J_{ij} = 8 t_i^2 \left\{ \frac{U_i + U_j}{(U_i + U_j)^2 - 4(\epsilon_i - \epsilon_j)^2} \right\} \tag{7}$$

is the antiferromagnetic exchange coupling between $\hat{S}_i$ and $\hat{S}_j$. In most of the following discussion, to avoid too many parameters, we assume that the four dots are internally identical with $U_i \equiv U$ and $\epsilon_i \equiv \epsilon$. Therefore, since $\epsilon = -U/2$, one then has $J_0 = 8\tau^2/U$, $J_1 = J_{12} = 4t_1^2/U$, and $J_2 = J_{23} = 4t_2^2/U$.

For the system considered in this paper, it is convenient to define two subsystems, one formed by the central dot (subsystem $\mathbb{CD}$) and the other formed by the three side dots (subsystem $\mathbb{SD}$). When there are no interactions between spins on the same subsystem, the ground state of the whole TQQD has a total spin $S_{\rm tot} = |S_{\mathbb{CD}m} - S_{\mathbb{SD}m}|$ in light of the Lieb-Mattis theorem [61]. Here, $S_{\mathbb{CD}m}$ ($S_{\mathbb{SD}m}$) is the maximum possible spin on subsystem $\mathbb{CD}$ ($\mathbb{SD}$). Thus the ground state of the isolated TQQD will have a total spin $S_{\rm tot} = 1$. If only t_1 is taken into account, the isolated TQQD model could be illustrated by $J_1 \hat{S}_{\mathbb{CD}} \cdot \hat{S}_{\mathbb{SD}}$, where $\hat{S}_{\mathbb{CD}}$ ($\hat{S}_{\mathbb{SD}}$) is the spin operator of subsystem $\mathbb{CD}$ ($\mathbb{SD}$). Since the antiferromagnetic exchange couplings between the central dot and the side dots are identical, one has $\hat{S}_{\mathbb{SD}} = \sum_{i=2}^{4} \hat{S}_i$. The eigenstates of this system then could be obtained by a combination of the spin operators of the two subsystems $\hat{S}_{\rm tot} = \hat{S}_{\mathbb{CD}} + \hat{S}_{\mathbb{SD}}$, where the corresponding eigenvalues could be acquired by virtue of $J_1 \hat{S}_{\mathbb{CD}} \cdot \hat{S}_{\mathbb{SD}} = J_1 (\hat{S}^2_{\rm tot} - \hat{S}^2_{\mathbb{CD}} - \hat{S}^2_{\mathbb{SD}})/2$:

$$E_{S_{\rm tot} = S_{\mathbb{SD}} - \frac{1}{2}} = -\frac{5}{4} J_1. \tag{8}$$

If t_2 is also considered, the competition between t_1 and t_2 may result in QPTs, as will be discussed in the following.

We calculate the conductance $G(T)$ through the TQQD at temperature T using the Landauer formula [62,63]:

$$\begin{aligned} G(T) &= \sum_\sigma G_\sigma(T) \\ &= G_0 \sum_\sigma \int_{-\infty}^{+\infty} \pi \Gamma \left[-\frac{\partial f(\omega)}{\partial \omega} \right] A_{1\sigma}(\omega, T) d\omega. \end{aligned} \tag{9}$$

Here, $G_0 = 2e^2/h$ is the conductance quantum, ω is the energy variable, and $f(\omega) = 1/[1 + \exp(\omega/T)]$ is the Fermi-Dirac distribution function. $A_{1\sigma}(\omega, T)$ is the LDOS of the central dot at temperature T, with $A_{1\sigma}(\omega, T) = -\frac{1}{\pi}\mathrm{Im}G_{11\sigma}(\omega, T)$, and $G_{11\sigma}(\omega, T)$ is the Fourier transformation of the diagonal retarded Green's function. In the following discussion, we set the Fermi energy at $\omega = 0$; thus G_σ at zero temperature in the limit of zero bias is determined by the behavior of $A_{1\sigma}(\omega, T)$ at the Fermi level:

$$G_\sigma(T = 0) = \pi\Gamma G_0 A_{1\sigma}(\omega = 0, T = 0). \tag{10}$$

To improve the precision of the LDOS at finite temperature, we employ a procedure referring to the full density matrix of the whole system, which is denoted as FDM-NRG [64].

The temperature-dependent entropy $S_{\mathrm{TQQD}}(T)$ and local magnetic moment $\mu^2(T)$ of the TQQD are defined as the contribution to the total entropy and magnetic moment for the whole system, respectively:

$$S_{\mathrm{TQQD}}(T) = \frac{E - F}{T} - \frac{(E - F)_0}{T}, \tag{11}$$

$$\mu^2(T) = \chi_{\mathrm{TQQD}}(T)k_B T/(g\mu_B)^2 = \langle S_z^2\rangle - \langle S_z^2\rangle_0. \tag{12}$$

Here, $E = \langle H\rangle = \mathrm{Tr}(He^{-H/(k_BT)})$ and $F = -k_BT\ln\mathrm{Tr}(e^{-H/(k_BT)})$, which are the total energy and free energy of the whole system, respectively. $\chi_{\mathrm{TQQD}} = C/T$ is the contribution of the TQQD to the total magnetic susceptibility following the Curie law, where $C = (g\mu_B)^2 S_{\mathrm{tot}}(S_{\mathrm{tot}} + 1)/3$ is the Curie constant. k_B is Boltzmann's constant, g is the electric gyromagnetic factor, and μ_B is the Bohr magneton. Finally, the subscript 0 in $\frac{(E-F)_0}{T}$ and $\langle S_z^2\rangle_0$ refers to the value which belongs to the system where the TQQD is absent. It is noted here that for the sake of simplicity, we set $k_B \equiv 1$; hence the temperature is also given in units of energy.

IV. RESULTS AND DISCUSSION

A. A singular two-stage Kondo effect: Role of t_1 without t_2

Regular Kondo effect. In the following discussion, we choose W_b as the energy unit, which is about several eV in a typical metal electrode. The strongly correlated regime is described by $U = 10\Gamma$. Let us first focus on the case where t_2 is absent. In Fig. 2(a), we depict the linear conductance at nearly zero temperature $G(T \approx 0)$ as a function of t_1 with fixed $U = 0.1$. When t_1 is absent, $G(T \approx 0)/G_0$ reaches its unitary limit of 1.0. Because in this case the present model maps to a single-impurity Anderson model, the electrons in dot 1 are likely to form a spin singlet with those in the electrode. As a result, the Kondo effect is generated, and a peak at $\omega = 0$ in the normalized LDOS of electrons in dot 1 [$\pi\Gamma A_1(\omega)$, i.e., the transmission coefficient] reaches its maximum; see $t_1 = 0.0$ in Fig. 2(b).

Two-stage Kondo effect regime. When t_1 turns on, it induces an effective antiferromagnetic exchange coupling $J_1 = 4t_1^2/U$, which is enhanced as t_1 increases, reflected by the spin-spin correlation function $\langle S_1S_2\rangle$; see Fig. 2(c). On the other hand, electrons on different side dots may be organized in a parallel manner due to the interdot RKKY interaction J_{RKKY} mediated by t_1 [cf. $\langle S_2S_3\rangle$ in Fig. 2(c)]. In this process, $G(T \approx 0)/G_0$ decreases to zero continuously, because

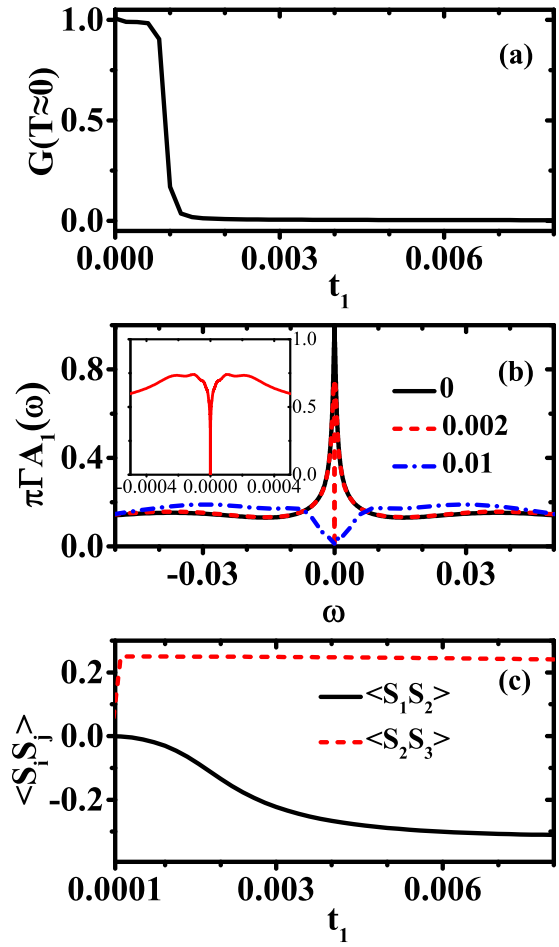

FIG. 2. (a) Linear conductance at nearly zero temperature, $G(T \approx 0)$, as a function of t_1. (b) Normalized LDOS of electrons in dot 1, $\pi\Gamma A_1(\omega)$, i.e., the transmission coefficient, for various t_1. (c) Spin-spin correlation $\langle S_iS_j\rangle$ between dots i and j at nearly zero temperature as a function of t_1. $\langle S_1S_2\rangle = \langle S_1S_3\rangle = \langle S_1S_4\rangle$, and $\langle S_2S_3\rangle = \langle S_3S_4\rangle = \langle S_4S_2\rangle$. Inset in (b): $\pi\Gamma A_1(\omega)$ for $t_1 = 0.002$, showing a considerable split in the Kondo peak. Here, $G(T \approx 0)$ and $\pi\Gamma A_1(\omega)$ are described in units of G_0. The other parameters are given by $\Gamma = 0.01$, $U = 0.1$, $\epsilon = -U/2$, and $t_2 = 0$.

the antiferromagnetic coupling between subsystems $\mathbb{CD}$ and $\mathbb{SD}$ suppresses the Kondo singlet and thus the Kondo peak splits and decreases gradually [cf. $t_1 = 0.002$ and $t_1 = 0.01$ in Fig. 2(b) and the inset]. One notices that in the large-t_1 regime, $\langle S_1S_2\rangle$ could not reach the ideal value of $-3/4$, for there are still some possibilities of electrons on dot 1 forming spin singlets with those on dots 3 and 4.

One of the most interesting behaviors may be that of the thermodynamical properties. Related results are depicted in Fig. 3, where we show the temperature-dependent linear conductance $G(T)$, the local magnetic moment $\mu^2(T)$, and the entropy $S_{\mathrm{TQQD}}(T)$ for the TQQD, as well as $\langle S_iS_j\rangle$ between dots i and j in terms of different t_1 in Figs. 3(a)–(d), respectively. The uppermost curve in Fig. 3(a) is for small $t_1 = 0.0001$. When $T/\Gamma \gg 1$ and $T/U \geqslant 1$, $G(T)$ is near zero for all t_1, because in this energy scale, local electrons are independent, and the influence of U, which favors a singly occupied state in each dot, is smeared out by temperature. As

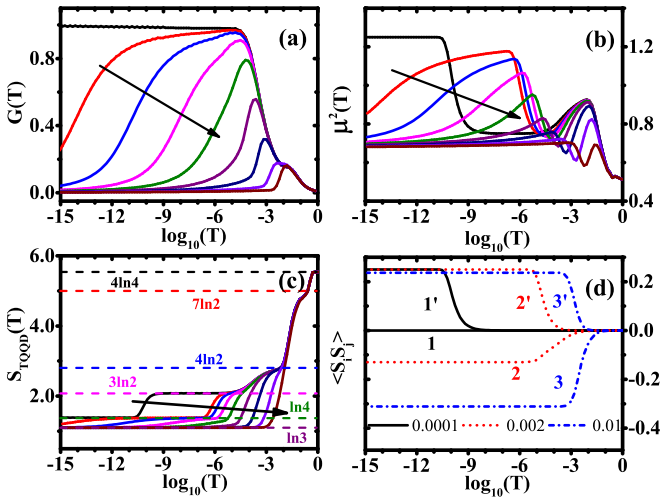

FIG. 3. (a) Linear conductance $G(T)$, (b) local magnetic moment $\mu^2(T)$, and (c) entropy $S_{\rm TQQD}(T)$ for the TQQD as functions of temperature T in terms of different t_1. The curves along the black arrow are for $t_1 = 0.0001, 0.001, 0.0012, 0.0015, 0.002, 0.003, 0.005, 0.01$, and 0.02, respectively. (d) $\langle S_i S_j\rangle$ between dots i and j vs $\log_{10}(T)$ for $t_1 = 0.0001$, 0.002, and 0.01. Curves 1–3 in (d) are for $\langle S_1 S_2\rangle$, whereas $1'$–$3'$ are for $\langle S_2 S_3\rangle$. The remaining parameters are the same as in Fig. 2.

a result, states $|0\rangle$, $|\uparrow\rangle$, $|\downarrow\rangle$, and $|2\rangle$ in each dot are equally probable. Each dot then contributes $1/8$ to $\mu^2(T)$ and $\ln 4$ to $S_{\rm TQQD}(T)$, resulting in total quantities $\mu^2(T) \approx 1/2$ and $S_{\rm TQQD}(T) \approx 4\ln 4$, and $\langle S_i S_j\rangle$ reads zero; see Figs. 3(b)–(d). As T decreases to the regime $\Gamma < T \leqslant U$, U starts to play an important role, and thus states $|0\rangle$ and $|2\rangle$ are suppressed. Each dot then contributes $1/4$ to $\mu^2(T)$ and $\ln 2$ to $S_{\rm TQQD}(T)$, leading to $\mu^2(T) \approx 1.0$ and $S_{\rm TQQD}(T) \approx 4\ln 2$. Transport in this regime is mainly dominated by the cotunneling process [65]; hence one may observe a small plateau in $G(T)$. Also, one notices a narrow plateau in $S_{\rm TQQD}(T)$ between $4\ln 4$ and $4\ln 2$, because the cotunneling magnitudes are different between subsystems $\mathbb{CD}$ and $\mathbb{SD}$. $\mathbb{CD}$ first contributes to the cotunneling process due to direct connection with the electrodes; hence in this regime, $S_{\rm TQQD}(T) \approx \ln 2 + 3\ln 4 = 7\ln 2$. As $T_{K1} < T \leqslant \Gamma$, the effect of Γ becomes quite momentous, and a spin singlet is then generated between electrons in $\mathbb{CD}$ and those in the conduction baths; hence $G(T)$ increases gradually to its unitary limit due to the regular Kondo effect. In such a case, the spin on dot 1 is quenched and has no contribution to $\mu^2(T)$, bringing $\mu^2(T) \approx 3/4$ and $S_{\rm TQQD}(T) \approx \ln 1 + 3\ln 2$. Here, T_{K1} is the first-stage Kondo temperature, which could be estimated by the following physical picture. For small t_1, the present model is similar to the single-impurity Anderson model, and the Kondo temperature could be captured by Haldane's expression [66]:

$$T_{K1} = U\sqrt{\rho_0 J_K}\exp(-1/\rho_0 J_K), \tag{13}$$

where $\rho_0 J_K = 8\Gamma/\pi U$ is the effective Kondo coupling between the conduction band and subsystem $\mathbb{CD}$. For fixed $U = 0.1$ and $\Gamma = 0.01$, $T_{K1} = 1.01\times 10^{-3}$. Below T_{K1}, the Kondo effect holds, and a broad platform exists in $\mu^2(T)$. However, when $T \ll T_{K1}$, we find two new energy scales which have been less discussed in the previous literature. As can be seen in Fig. 3(b), when T decreases to the scale of $T_{\rm RKKY} \approx 10^{-10}$, $\mu^2(T)$ increases again. Because in this regime the RKKY interaction between different side dots mediated by t_1 becomes significant, the local spins on subsystem $\mathbb{SD}$ are then arranged ferromagnetically, as confirmed by $\langle S_2 S_3\rangle$ growing to about 0.25 in Fig. 3(d). The TQQD locks into a high-spin state with a total spin $S_{\rm tot} = S_{\mathbb{SD}} = 3/2$, giving $\mu^2(T) = S_{\rm tot}(S_{\rm tot}+1)/3 = 5/4$, and $S_{\rm TQQD}(T)$ decreases to about $\ln(2S_{\rm tot}+1) \approx \ln 4$. Note that in this case the local spin on dot 1 still forms a singlet with those on the electrodes and has no contribution to $\mu^2(T)$ or $S_{\rm TQQD}(T)$.

With increasing t_1, the Kondo effect is suppressed gradually; thus $G(T)$ at low temperature decreases. Also, one notices that the temperature where $G(T)$ weakens to zero increases, indicating that the temperature window where the Kondo effect occurs becomes more and more narrow; see along the black arrow in Fig. 3(a). During this process, the spin of subsystem $\mathbb{SD}$ is partially screened by the heavy-fermion system constituted by the $\mathbb{CD}$ spin through J_1 at a certain temperature T_{K2}, giving a residual spin of $S_{\rm tot} = S_{\mathbb{SD}} = 1$. Hence $\mu^2(T)$ and $S_{\rm TQQD}(T)$ reduce to $2/3$ and $\ln 3$ when $T \leqslant T_{K2}$, respectively. This two-stage screening process is distinguished from the regular two-stage Kondo effect observed in a SDQD system, where the first screening is directly followed by the second one [33,67]. One notices that T_{K2} increases with growing t_1, and this screening is not accompanied by the Kondo resonance in $G(T)$ and $\pi\Gamma A_1(\omega)$, whereas it is along with the suppression of the Kondo effect [cf. Figs. 2(a) and 2(b)]. As a result, the conductance is zero for $T < T_{K2}$.

Molecular-orbital regime. When t_1 is large enough with $t_1 \gg T_{K1}$, the antiferromagnetic exchange coupling between subsystems $\mathbb{CD}$ and $\mathbb{SD}$ is extremely strong, which then suppresses the Kondo resonance at low temperature; hence only the cotunneling process survives in $G(T)$. Equivalently speaking, a local spin singlet forms between the central dot and one of the side dots, whereas the remaining two side dots constitute a spin triplet at $T \sim t_1$ with residual spin $S_{\rm tot} = S_{\mathbb{SD}} = 1$ [see Figs. 2(c) and 3(d)]; thus $\mu^2(T) \approx 2/3$ and $S_{\rm TQQD}(T) \approx \ln 3$ hold in a broad regime of T.

Relation between T_{K2} and t_1. To form a deep understanding of the above temperature scales, we depict T_{K2} and its fitting function versus t_1 in Fig. 4(a). Here, T_{K2} is captured from our NRG data and is defined by the temperature corresponding to the half maximum of $\mu^2(T)$ where the TQQD decreases from the high-spin state to its minimal value at low temperature. One may see that T_{K2} increases exponentially as t_1 sweeps upwards and could be illustrated by a function of T_{K1} and J_1:

$$T_{K2} = c_1 T_{K1} e^{-c_2 T_{K1}/J_1}. \tag{14}$$

Here, the fitting parameters are given by $c_1 = 0.004$ and $c_2 = 0.586$. One finds that the fitting function is consistent with our NRG results, implying that the above phenomenon that occurs in $G(T)$ and $\mu^2(T)$ is in essence a two-stage Kondo effect. However, singular behaviors could be identified. As is known, in typical SDQD systems the fitting parameters c_1 and c_2 are some constants of the order of 1 [33,67], which are quite different from ours. In our present model, the two Kondo screenings are separated by a RKKY temperature scale $T_{\rm RKKY}$.

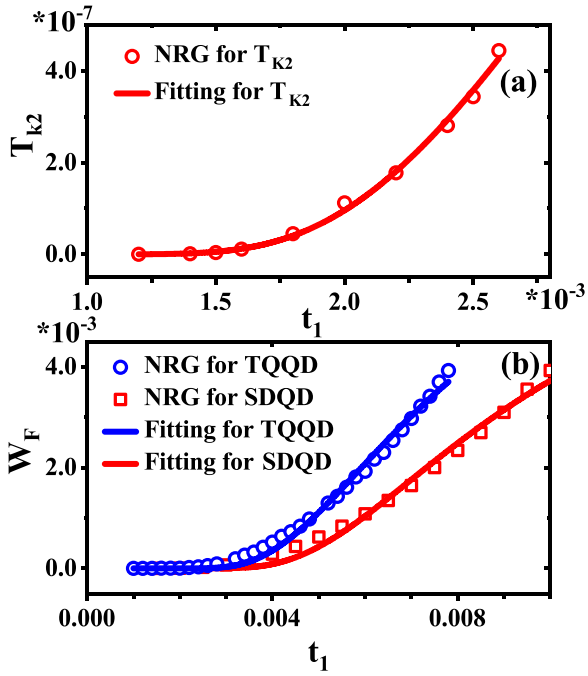

FIG. 4. (a) T_{K2} and (b) W_F for both the TQQD and the SDQD systems as functions of t_1. Scatterplots are captured from our NRG data, while the solid curves are the fitting functions for T_{K2} and W_F. The other parameters are the same as in Fig. 2.

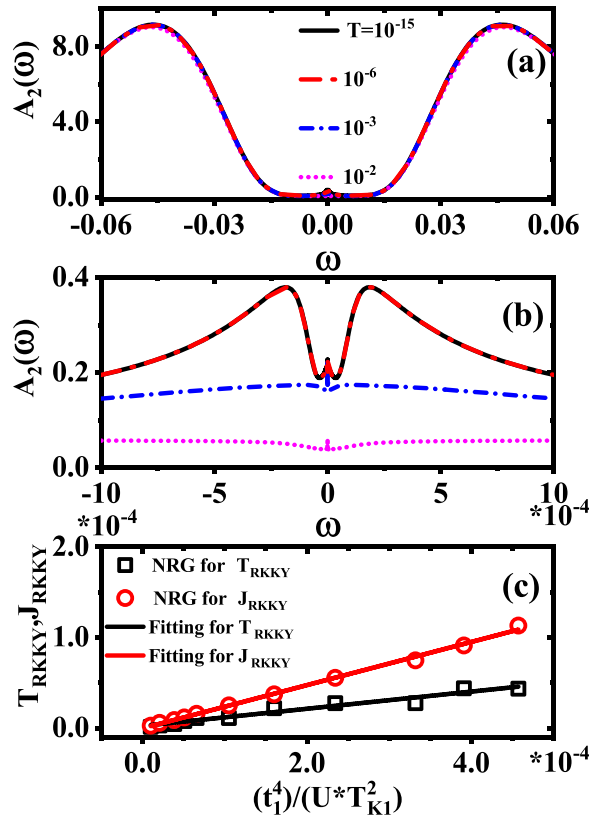

FIG. 5. (a) The LDOS of the side dots $A_2(\omega)$ at different temperatures and (b) $A_2(\omega)$ in an expanded scale around the Fermi level for $t_1 = 0.003$. (c) The RKKY temperature $T_{\rm RKKY}$ extracted from $\mu^2(T)$ in Fig. 3(b), the location of the RKKY peak $J_{\rm RKKY}$ in $A_2(\omega)$, and their fitting functions vs $t_1^4/(UT_{K1}^2)$. The other parameters are the same as in Fig. 2.

Thus T_{K2} becomes extremely low compared with T_{K1}, and c_1 is more lower than that in the SDQD structure. Furthermore, since in our model three side dots are connected to the central dot simultaneously, the effective coupling between the central dot and one of the side dots will be lower than that in the SDQD system with the same quantity of the tunneling rate, and thus c_2 is also slightly smaller than order 1. We note that there should be theoretically a second drop occurring at T_{K2} for $t_1 = 0.0001$ [cf. Figs. 3(a)–(c)]. However, in such a case, Eq. (14) gives $T_{K2} \to 0$; hence it is extremely difficult to capture in both related experiments and theoretical simulations.

Relation between W_F and t_1. It is noticed that in side-coupled quantum dot systems, the second Kondo screening related to T_{K2} is always associated with the Fano effect, which results from the interference between the direct and indirect conduction pathways [33,68]. As a result, a Fano antiresonance may appear in the LDOS of the quantum dot embedded in the direct conduction pathway between the source and drain electrodes; such is also the case for our results presented in Fig. 2(b). It is quite interesting to study the evolution of the Fano antiresonance and compare it with that of T_{K2}. In Fig. 4(b), we describe the width of the Fano dip W_F and its fitting function as functions of t_1. Here, W_F is defined by the full width at half maximum of the central valley. We find that W_F could also be illustrated by an exponential function of t_1 and the width of the Kondo peak W_K, which is extracted when t_1 is absent:

$$W_F = c_3 W_K e^{-c_4 W_K/J_1}, \tag{15}$$

with $c_3 = 6.537$ and $c_4 = 2.462$. Quite interestingly, these parameters are very close to those in the SDQD system. As is illustrated in Fig. 4(b), for a SDQD, W_F could also be described by Eq. (15), where c_3 and c_4 are given by 6.754 and 1.610, respectively. Therefore the number of side dots affects the width of the Fano dip in a very gentle way, especially when t_1 is small, whereas it affects the order of T_{K2} intensely.

Relation between $T_{\rm RKKY}$ and $J_{\rm RKKY}$. From the above discussion, one knows that when T decreases to $T_{\rm RKKY}$, the TQQD locks into a high-spin state for small t_1, which stems from the RKKY interaction $J_{\rm RKKY}$ between different side dots. It is interesting to clarify the relation between $J_{\rm RKKY}$ and $T_{\rm RKKY}$. As an example, we show the LDOS for one of the side dots $A_2(\omega)$ at different temperatures with fixed $t_1 = 0.003$, and its enlarged scale around $\omega = 0$ in Figs. 5(a) and 5(b), respectively. One finds two broad Coulomb peaks located at about $\omega = \pm U/2$ for all temperatures. From the enlarged $A_2(\omega)$, one notices two additional peaks between the Fermi level and the Coulomb peaks. They are the so-called RKKY peaks [69,70], which exist only when $T \leqslant T_{\rm RKKY}$ [cf. Fig. 5(b)]. Here, the RKKY peak refers to the process of annihilating (creating) an electron from (on) the many-body states of the side dots with antiparallel spin configuration, where at least two electrons on two of the side dots have parallel spin configuration, mediated by t_1. One then could identify the strength of the RKKY interaction $J_{\rm RKKY}$ from the location of the RKKY peak, which is plotted in Fig. 5(c). It is seen that $J_{\rm RKKY}$ grows in a power

series manner as t_1 increases, and can be fitted by a function of t_1:

$$J_{\mathrm{RKKY}} = c_5 t_1^4/\left(UT_{K1}^2\right), \tag{16}$$

with $c_5 = 0.24$. Meanwhile, we also depict T_{RKKY} and its fitting function varying with t_1 in Fig. 5(c). Here, T_{RKKY} is defined by the temperature referring to the half maximum of $\mu^2(T)$ where the TQQD enters into the high-spin state after the first Kondo screening [cf. Fig. 3(b)]. We find that T_{RKKY} could also be illustrated by a function of the order of t_1^4:

$$T_{\mathrm{RKKY}} = c_6 t_1^4/\left(UT_{K1}^2\right), \tag{17}$$

with $c_6 = 0.10$. We argue that these behaviors could be attributed to the following picture. For the parallel multi-quantum-dot systems, the RKKY interaction J_{RKKY} is mediated by the effective Kondo couplings between the conduction band and quantum dots and is of the order of Γ^2, i.e., thus τ^4, with $J_{\mathrm{RKKY}} \propto U(W_b J_K)^2 \propto \Gamma^2/U$ [71]. In the limit of noninteracting electrons in the central dot with $U = 0$, the hybridization function between the central and the side dots $\Gamma_{c\text{-}s}$ is given by $\Gamma_{c\text{-}s}(\omega) = \pi A_1^0(\omega) t_1^2$, where $A_1^0(\omega)$ denotes the spectral function of the central dot without t_1:

$$A_1^0(\omega) = \frac{1}{\pi}\frac{\Gamma}{(\omega-\epsilon)^2+\Gamma^2}. \tag{18}$$

In this way, the relation between $\Gamma_{c\text{-}s}(\omega)$ and t_1 becomes similar to that between Γ and τ. If the Coulomb repulsion in the central dot is strong, such as in the case of our present model, $\Gamma_{c\text{-}s}$ becomes more complex, since the Green's function of the central dot is then given by a function of ϵ, t_1, Γ, and the self-energy of the dots. Nevertheless, the second Kondo screening corresponds to a Kondo effect due to J_1 between a spin-3/2 impurity and a Fermi liquid, which has an effective bandwidth $\widetilde{W}_b \sim T_{K1}$ and a LDOS at the Fermi level $\widetilde{A}_1^0(\omega = 0) \sim 1/(\pi T_{K1})$ [67]. As a result, for low frequencies, $\Gamma_{c\text{-}s} \propto t_1^2/T_{K1}$, and $J_{\mathrm{RKKY}} \propto t_1^4/(UT_{K1}^2)$. Furthermore, one notices that in the parallel multi-quantum-dot systems, it is found that $J_{\mathrm{RKKY}} = cT_{\mathrm{RKKY}}$, with c being a constant of order 1 [71]. In our present model, we find that this relation is also valid. Furthermore, it is notable that a similar two-peak structure of $\mu^2(T)$ was observed in quantum dot arrays with a star configuration [72]; however, neither of the peaks was identified as the contribution of the RKKY interaction, and the underlying physical picture was not shown.

B. A QPT between different singular two-stage Kondo behaviors: Effect of t_2 with intermediate $t_1 \sim T_{K1}$

From the above discussion, one observes a crossover from the fully conductance state to the zero-conductance state when t_1 increases; however, the reappearance of the Kondo effect may occur when t_2 is applied if $t_1 \sim T_{K1}$, accompanied by two first-order QPTs. In Fig. 6, we illustrate $\pi\Gamma A_1(\omega)$ in terms of different t_2, the linear conductance $G(T)$, the charge occupation number $\langle n_i\rangle$ of subsystem i ($i = \mathbb{CD}, \mathbb{SD}$), and the spin correlation $\langle S_i S_j\rangle$ at nearly zero temperature as functions of t_2 with fixed $t_1 = 0.002$. As t_2 increases, the split Kondo peaks move toward the Fermi level. When t_2 is large enough, the Kondo peak locates at $\omega = 0$ and reaches its unitary limit, indicating a full conductance; see Fig. 6(a). Evolution of

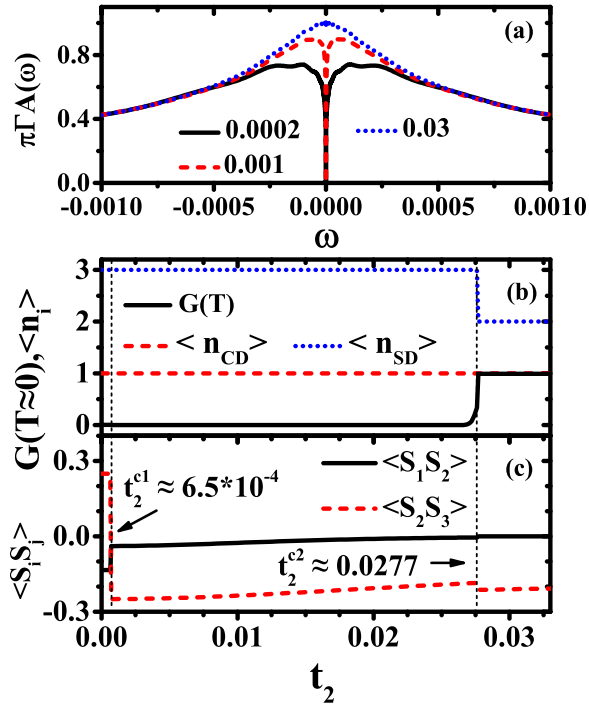

FIG. 6. (a) $\pi\Gamma A_1(\omega)$ for various t_2 at $T \approx 0$. (b) $G(T \approx 0)$ and the charge occupation number on subsystems $\mathbb{CD}$ $\langle n_{\mathbb{CD}}\rangle$ and $\mathbb{SD}$ $\langle n_{\mathbb{SD}}\rangle = \sum_{i=2}^{4}\langle n_i\rangle$ as functions of t_2. (c) $\langle S_i S_j\rangle$ at nearly zero temperature as a function of t_2. The vertical black dashed lines in (b) and (c) describe the two critical points of the QPTs. Here, t_1 is fixed at 0.002, and the remaining parameters are the same as in Fig. 2.

$G(T \approx 0)$ versus t_2 is presented in Fig. 6(b); one finds that it jumps from 0.0 to 1.0 around $t_2 = 0.0277$. However, as a matter of fact, the zero-conductance state covers two different quantum phases. As shown in Figs. 6(b) and 6(c), when t_2 is small, each dot remains half filled, and the total charge number of the TQQD reads $\langle N_{\mathrm{tot}}\rangle = \langle n_{\mathbb{CD}}\rangle + \langle n_{\mathbb{SD}}\rangle = 4.0$. In this case, electrons on dot 1 and those on the side dots are arranged antiferromagnetically due to t_1, whereas those on different side dots are organized in a parallel manner; see Fig. 6(c). The ground state of subsystem $\mathbb{SD}$ is a spin quadruplet. We note that when t_2 turns on, the exchange interactions between different side dots include both the ferromagnetic RKKY interaction mediated by t_1 and the direct antiferromagnetic exchange (DAE) interaction induced by t_2 with $J_2 = 4t_2^2/U$ [cf. Eq. (7)]. As t_2 increases, the DAE interaction competes with the RKKY interaction, so that at the first critical point $t_2^{c1} \approx 6.5 \times 10^{-4}$, the spin correlation between different side dots $\langle S_2 S_3\rangle$ drops abruptly to negative values, indicating a first-order QPT. The ground state of subsystem $\mathbb{SD}$ then goes into a magnetic frustration phase, which is dominated by those many-body states with two of the side dots forming a spin singlet while the remaining one generates another spin singlet with the central dot. Hence electrons still could not transmit through the TQQD. Here, t_2^{c1} satisfies that $J_2 = J_{\mathrm{RKKY}}$, viz., $4(t_2^{c1})^2/U = 0.24t_1^4/(UT_{K1}^2)$, giving $t_2^{c1} \approx 9.79 \times 10^{-4}$. Due to magnetic frustration and the temperature being not accurately at zero, the numerical result of t_2^{c1} diverges mildly from the theoretical one.

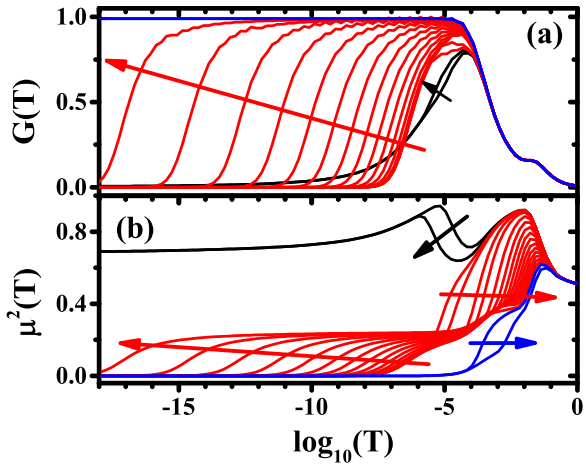

FIG. 7. Temperature-dependent (a) $G(T)$ and (b) $\mu^2(T)$ for the TQQD. The three different phases in each panel are distinguished by black, red, and blue, respectively. Curves in (a) and (b) along the black arrow are for $t_2 = 0.0002$ and 0.0006; curves along the red arrow are for $t_2 = 0.0008$, 0.001, 0.002, and 0.003–0.027 in steps of 0.002; and curves along the blue arrow are for $t_2 = 0.028$ and 0.030, respectively. The remaining parameters are the same as in Fig. 6.

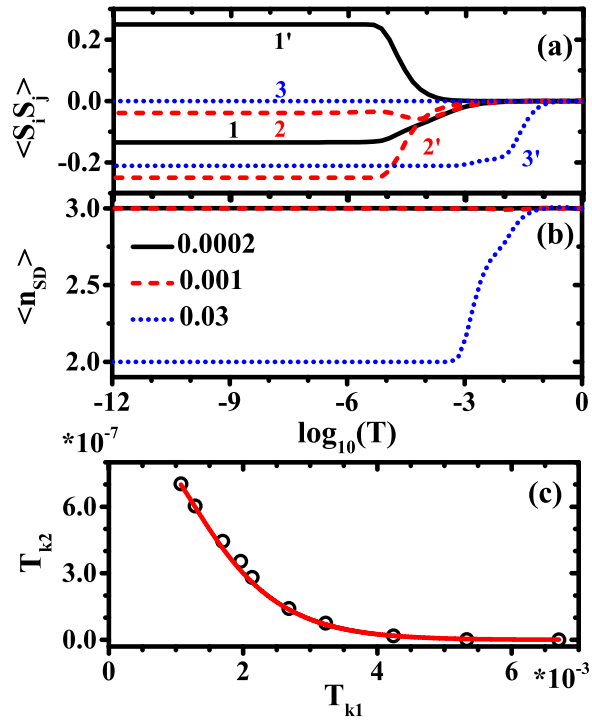

FIG. 8. (a) $\langle S_i S_j \rangle$ and (b) $\langle n_{\mathbb{SD}} \rangle$ as functions of temperature. Curves in (a) and (b) are for $t_2 = 0.0002$, 0.001, and 0.03, respectively. Curves 1–3 in (a) are for $\langle S_2 S_3 \rangle$, whereas curves 1′–3′ are for $\langle S_1 S_2 \rangle$. Furthermore, since $\langle n_{\mathbb{CD}} \rangle$ holds at 1.0 in all temperature regimes, we have not shown it here. The remaining parameters are the same as in Fig. 2.

The above phase corresponds to the lowest energy for a region of intermediate values of t_2; however, it suffers another QPT upon increasing this parameter further. As t_2 exceeds another critical point $t_2^{c2} \approx 0.0277$, $\langle n_{\mathbb{SD}} \rangle$ changes abruptly to 2.0, suggesting another first-order QPT. In such a situation, two of the side dots are singly occupied by electrons with antiparallel configuration, and both of them decouple from the central dot, while the remaining side dot is empty. The present model then maps to a single-impurity Anderson model with a single electron, and the Kondo peak recovers within the transmission coefficient at low temperature [cf. $t_2 = 0.03$ in Figs. 6(a) and 6(b)]. t_2^{c2} is just the point where the energy level of the magnetic frustration phase degenerates with that of the $\langle n_{\mathbb{SD}} \rangle = 2.0$ phase.

Temperature-dependent physical quantities are depicted in Figs. 7 and 8. For small $t_2 \leqslant t_2^{c1}$, e.g., $t_2 = 0.0002$ and 0.0006, the thermodynamical properties are similar to the case without t_2 [cf. Figs. 3, 7, and 8]. The increasing t_2 seems to not affect T_{K2}, whereas it does affect T_{RKKY}, because the DAE interaction impairs the RKKY interaction. For intermediate values of t_2 such that $t_2^{c1} < t_2 \leqslant t_2^{c2}$, e.g., t_2 illustrated by the red curves in Fig. 7(a), the line shape of $G(T)$ is different from those of $t_2 \leqslant t_2^{c1}$, but a broad highland also exists in $G(T)$ in the regime $T_{K1} \geqslant T > T_{K2}$. Meanwhile, one notices that screening of $\mu^2(T)$ also takes place in two stages, indicating a novel two-stage Kondo effect. With decreasing temperature, there is a first drop at the scale of T_{K1} followed by a plateau with $\mu^2(T) \approx 1/4$. Because when $t_2 > t_2^{c1}$ the DAE interaction overwhelms the RKKY interaction, the high-spin state with $S_{\mathbb{SD}} = 3/2$ induced by the RKKY interaction disappears. Instead, two of the side dots form a spin singlet, and the central one generates a Kondo singlet with an electron in the conduction band; see Fig. 8(a). Therefore only the remaining side dot contributes 1/4 to $\mu^2(T)$. A second drop occurs at a much lower scale T_{K2}, where a spin singlet develops between the remaining side dot and the central one. The present structure maps to a SDQD model, and the spin on the remaining side dot is screened by the coupling between the central dot and the side one. As a result, the total magnetic moment vanishes with $\mu^2(T) \to 0$ as $T \to 0$. It is noticed that in this phase, T_{K1} becomes rather sensitive to the value of t_2, which increases with growing t_2. Because in this regime two of the side dots form a spin singlet, both the remaining side dot and the electrodes contribute to the screening of the local spin on subsystem $\mathbb{CD}$. This enhancement of T_{K1} then leads to the reduction of T_{K2}. In Fig. 8(c), we depict T_{K2} as a function of T_{K1} for $t_2^{c1} < t_2 \leqslant t_2^{c2}$. One finds that it could be simulated by a two-stage-Kondo-effect-type function,

$$T_{K2} = c_7 T_{K1} e^{-c_8 T_{K1}/J_1}, \tag{19}$$

with $c_7 = 0.0036$ and $c_8 = 0.633$, indicating that this Kondo screening is also a singular two-stage Kondo effect.

For large $t_2 > t_2^{c2}$, e.g., $t_2 = 0.028$ and 0.030, the Kondo effect recovers when $T \leqslant T_{K1}$; hence $G(T) \approx 1.0$ holds. In this section, two of the side dots form a spin singlet and decouple from the central dot, while the remaining side dot is empty, which is mentioned above [cf. Figs. 6(c) and 8(a)]. The local spin on subsystem $\mathbb{CD}$ is screened by electrons in the conduction band; hence $\mu^2(T) = 0$ at low temperature. It is worth noting that compared with the case $t_2 < t_2^{c2}$, where $\langle n_{\mathbb{SD}} \rangle \approx 3.0$ holds at all temperature scales, the state with $\langle n_{\mathbb{SD}} \rangle = 2.0$ only exists when $T < t_2$ [cf. Fig. 8(b)]. Thus, at high temperature, $\mu^2(T)$ is the same as the case $t_2 < t_2^{c2}$.

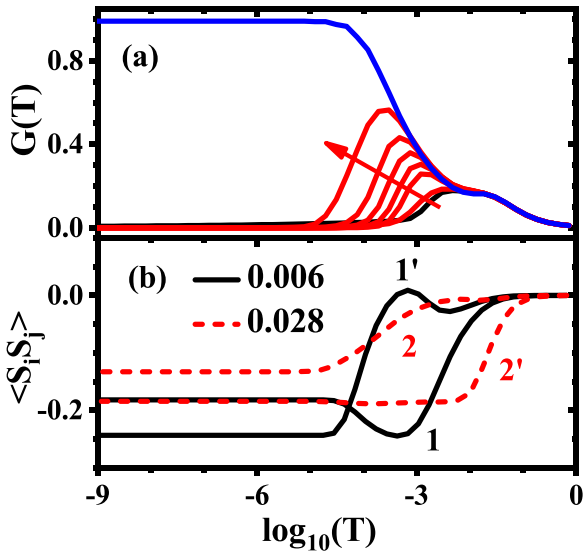

FIG. 9. (a) Temperature-dependent $G(T)$ through the TQQD. Curves for three different quantum phases are labeled by black, red, and blue severally, and are for $t_2 = 0.002$, 0.006, 0.012–0.028 in steps of 0.004, and 0.05, respectively, along the red arrow. (b) $\langle S_i S_j \rangle$ as a function of temperature T for $t_2 = 0.006$ (solid curves) and 0.028 (dashed curves), respectively. Curves 1 and 2 in (b) are for $\langle S_1 S_2 \rangle$, whereas curves $1'$ and $2'$ are for $\langle S_2 S_3 \rangle$. Here, $U = 0.1$, $\Gamma = 0.01$, $\epsilon = -U/2$, and $t_1 = 0.01$.

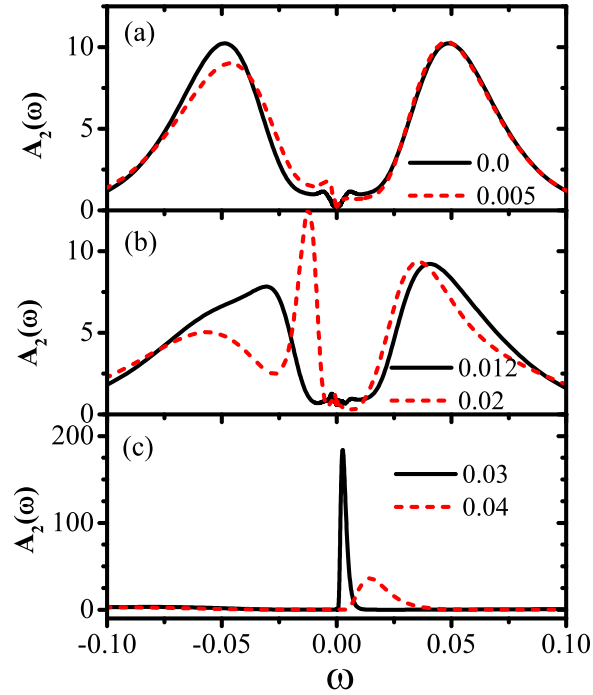

FIG. 10. (a)–(c) The LDOS of one of the side dots $A_2(\omega)$ in terms of different t_2. The remaining parameters are the same as in Fig. 9.

C. Robustness of the RKKY interaction and the partially recovered Kondo effect: Effect of t_2 with large $t_1 \gg T_{K1}$

For any fixed t_1, our numerical results show that there exist two QPTs as t_2 increases. If t_1 is small enough with $t_1 \ll T_{K1}$, these QPTs hardly affect the transport behaviors through the TQQD; hence we ignore them in our present discussion. On the other hand, if $t_1 \gg T_{K1}$, in the first and second quantum phases, $G(T)$ at low temperature is nearly zero, while it jumps to its unitary limit when t_2 moves across the second critical point, similar to the case of fixed $t_1 \sim T_{K1}$. Therefore in this section we focus our attention on two features, viz., the partially recovered Kondo effect and the interplay between $J_{\rm RKKY}$ and $J_{\rm DAE}$ characterized by the LDOS of subsystem $\mathbb{SD}$.

Temperature-dependent $G(T)$ through the TQQD is depicted in Fig. 9 with fixed $t_1 = 0.01$. For small $t_2 < t_2^{c1}$, e.g., $t_2 = 0.002$, the thermodynamical properties are similar to the case without t_2 [cf. Figs. 3(a) and 9(a)]. For intermediate values of t_2 such that $t_2^{c1} \leqslant t_2 < t_2^{c2}$ but $t_2 > t_1$, e.g., 0.012–0.028, a new small peak develops in $G(T)$ around $T \approx 10^{-3}$, which grows with increasing t_2. When $T \approx t_2$, the spin configurations between different side dots are dominated by antiferromagnetic style with negative $\langle S_2 S_3 \rangle$, whereas they nearly decouple from the central dot with $\langle S_1 S_2 \rangle \approx 0.0$; see, for example, $t_2 = 0.028$ in Fig. 9(b). Therefore, for $T < T_{K1} \approx 10^{-3}$, there are some possibilities for the electron on the central dot to form a spin singlet with that on the electrode, and the Kondo effect partially reappears. Comparing with these phenomena, one notices that for $t_2^{c1} \leqslant t_2 < t_2^{c2}$ but $t_2 < t_1$, the additional small peak in $G(T)$ is not obvious [cf. $t_2 = 0.006$ in Fig. 9(a)]. This behavior could be attributed to the fact that in this case the electron on the central dot generates a local spin singlet with the electron on one of the side dots at a higher temperature than the singlet between different side dots [cf. Fig. 9(b)]; hence around $T \approx T_{K1}$ the Kondo spin singlet is suppressed.

Since the RKKY interaction between different side dots $J_{\rm RKKY} \propto t_1^4$, for fixed large t_1, the order of $J_{\rm RKKY}$ is close to that of the Coulomb interaction; it is then an ideal prototype for discussing the interplay between $J_{\rm RKKY}$ and $J_{\rm DAE}$ in the LDOS. Related results are depicted in Fig. 10. When t_2 is absent, two pairs of energy peaks could be clarified in $A_2(\omega)$, both of which are symmetric to the Fermi level; see $t_2 = 0$ in Fig. 10(a). The broad pair are located at $\pm U/2$, which refer to the one-electron peak ($\epsilon = -U/2$) and the two-electron peak ($\epsilon + U$), respectively. The narrow pair are the RKKY peaks, which, as we may expect, are located at about $\pm 0.24 t_1^4/(U T_{K1}^2)$. When t_2 turns on, the spectral weight becomes asymmetric due to the electron-hole symmetry being broken [cf. $t_2 = 0.005$]. In this case, $J_{\rm DAE}$ reduces the probability of generating $J_{\rm RKKY}$, and thus the spectral weight contributed by $J_{\rm RKKY}$ decreases, which can be seen from the decreasing weight of the RKKY peak in the part $\omega > 0$. When t_2 exceeds t_2^{c1}, the RKKY peaks disappear, and instead there is another peak on the left side, $\omega < 0$; see $t_2 = 0.01$ in Fig. 10(b). This is because in this phase, the interdot exchange interaction is dominated by $J_{\rm DAE}$. With increasing t_2, the peak moves away with respect to the Fermi level, because $J_{\rm DAE}$ is enhanced; cf. $t_2 = 0.02$. When $t_2 > t_2^{c2}$, most of the spectral weight moves to the right side, suggesting a considerable reduction in the charge number of subsystem $\mathbb{SD}$; see $t_2 = 0.03$ in Fig. 10(c). The location of the peak refers to the energy needed to add an additional electron in subsystem $\mathbb{SD}$, which increases with growing t_2; thus one finds that it moves toward the right for larger t_2 [cf. $t_2 = 0.04$].

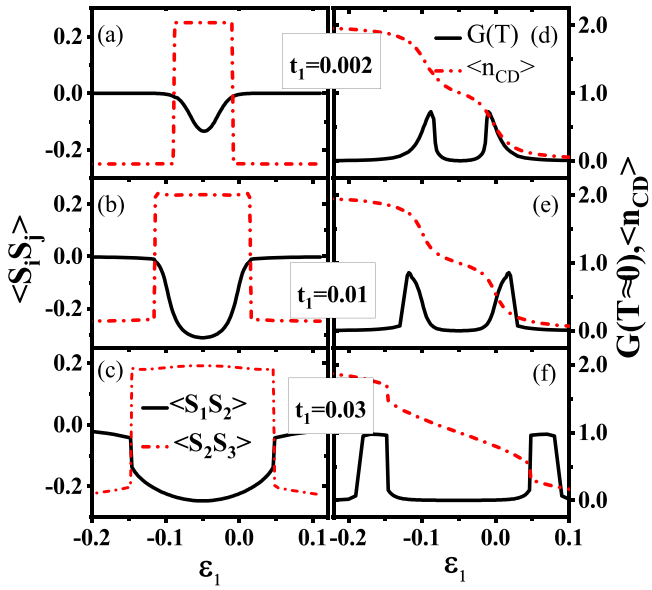

FIG. 11. (a)–(c) $\langle S_i S_j \rangle$ and (d)–(f) $G(T \approx 0)$ and $\langle n_{\mathbb{CD}} \rangle$ vs ϵ_1 at nearly zero temperature. The results correspond to $t_1 = 0.002$ [(a) and (d)], $t_1 = 0.01$ [(b) and (e)], and $t_1 = 0.03$ [(c) and (f)]. The remaining parameters are given by $U = 0.1$, $\Gamma = 0.01$, $\epsilon_2 = -U/2$, and $t_2 = 0$.

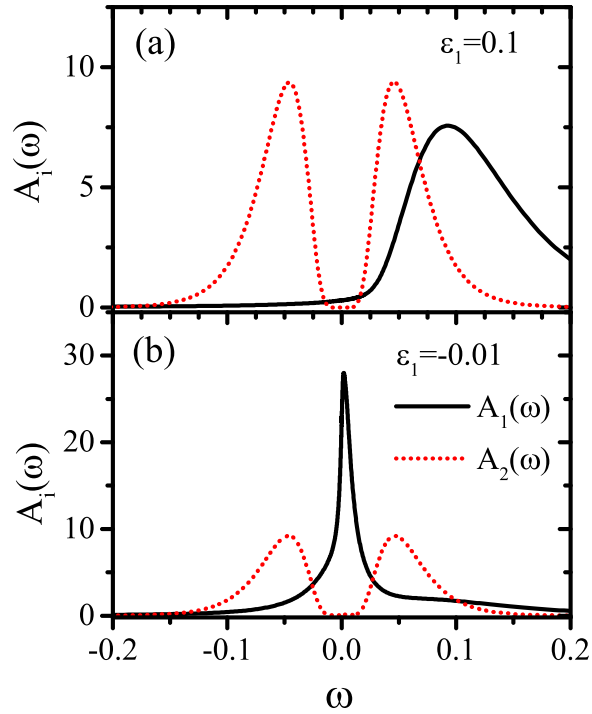

FIG. 12. (a) and (b) The LDOS of the quantum dots $A_i(\omega)$ ($i = 1, 2$) at nearly zero temperature in terms of different ϵ_1, with fixed $t_1 = 0.002$. The remaining parameters are the same as in Fig. 11.

D. A QPT from an antiferromagnetic to a ferromagnetic correlation among the side dots: Effect of ϵ_1 without t_2

We finish our discussion by analyzing the effect produced by changing the charge of the central dot, with the help of modifying its local level ϵ_1 via a gate potential. The left panels in Fig. 11 show $\langle S_i S_j \rangle$ at nearly zero temperature as a function of ϵ_1 for $t_1 = 0.002$ [Fig. 11(a)], 0.01 [Fig. 11(b)], and 0.03 [Fig. 11(c)], respectively, with fixed $\epsilon_2 = -U/2$ and $t_2 = 0$. It is seen that when t_2 is absent, charging subsystem $\mathbb{CD}$ triggers transitions from an antiferromagnetic correlation among the side dots to a ferromagnetic one, and then to an antiferromagnetic one. These QPTs are associated with Kondo regimes in $\mathbb{CD}$, which are characterized by peaks with maximum close to the unitary limit [cf. Figs. 11(d)–(f)]. The above behaviors are similar to those observed in a three-dot quantum gate, with a central dot connected to leads and laterally connected to two side quantum dots [73]. When ϵ_1 is high, e.g., $\epsilon_1 = 0.1$ for $t_2 = 0.002$, the central dot is nearly empty; thus the side spins decouple from the central one with $\langle S_i S_j \rangle \approx 0$ [cf. Figs. 11(a) and 11(d)]. In this case, the ground state of the isolated TQQD with $t_i = 0$ is a many-body state where the side spins are antiferromagnetically correlated. This behavior persists when dot 1 is connected to leads [73]. The spectral weight of $A_1(\omega)$ at the Fermi level is nearly zero; hence $G(T \approx 0) \approx 0$. Instead, there is a broad peak located at about ϵ_1, corresponding to the energy needed to add an additional electron on dot 1. $A_2(\omega)$ is symmetric with respect to the Fermi level, with two Coulomb peaks located at $\pm U/2$; see Fig. 12(a). As ϵ_1 sweeps to the Fermi energy, the Kondo effect occurs. This is because in this case, dot 1 is out of resonance and the effect of local repulsion in it can be neglected. This allows fourth-order spin-flipping processes between subsystems $\mathbb{CD}$ and $\mathbb{SD}$, which are characteristic of the Kondo effect [73,74]. This argument is confirmed by a sharp peak at the Fermi surface in $A_1(\omega)$, as is depicted in Fig. 12(b) with $\epsilon_1 = -0.01$. When ϵ_1 is low enough, e.g., $\epsilon_1 \ll 0$, dot 1 is almost fully occupied, and an analogous picture works due to the particle-hole symmetry; see Figs. 11(a) and 11(d). As t_1 increases, the ferromagnetically correlated regime of the side spins is enlarged. This is because the critical point around $\epsilon_1 = 0$ $(-U)$ also relates to the processes where the charge number increases from 0 (1) to 1 (2), and the level difference between these two states decreases as t_1 increases.

V. CONCLUSION

In conclusion, we have studied the quantum phase transition, the electronic transport, and the thermodynamical properties of a tetrahedral quadruple quantum dot system, connecting symmetrically to the source and drain electrodes. We concentrate on the two-stage Kondo effect, the RKKY interaction, the magnetic frustration, and their interplay in the strongly correlated limit. When t_2 is absent, the linear conductance $G(T)$ at zero temperature transits from its unitary limit to zero gradually as t_1 increases, due to the enhancing antiferromagnetism between the central and side subsystems. For intermediate values of t_1, a singular two-stage Kondo effect is revealed. The local spin of the TQQD is first screened by the effective Kondo coupling between the central dot and the electrodes at temperature T_{K1}, and then it locks into a high-spin state at T_{RKKY} due to the RKKY interaction J_{RKKY} between different side dots mediated by t_1. At a lower temperature T_{K2}, the high-spin state is then partially screened by the central spin through the exchange coupling induced by t_1.

The Kondo effect only exists in the regime $T_{K2} < T \leqslant T_{K1}$, with T_{K2} increasing as t_1 sweeps upwards. We demonstrate that T_{K2} could be illustrated by an exponential function of T_{K1}, but the orders of the fitting parameters are quite different from those in the SDQD structures. Both J_{RKKY} and T_{RKKY} could be described by power functions of $t_1^4/(UT_{K1}^2)$; hence J_{RKKY} is proportional to T_{RKKY}, similar to the parallel multi-quantum-dot structure. Surprisingly, the number of side dots affects the width of the Fano dip in a very gentle way, whereas it affects the order of T_{K2} significantly.

When t_2 turns on and the fixed $t_1 \sim T_{K1}$, the ground state of subsystem $\mathbb{SD}$ transits from a spin quadruplet to a magnetic frustration phase, and then to a singlet, through two first-order QPTs. In the quadruplet, electrons on the central dot form a singlet with those on one of the side dots; hence $G(T) = 0$ when $T < T_{K2}$. In the frustration phase, the quantum state of the TQQD is dominated by a state where electrons on two of the side dots generate a singlet, whereas an electron on the remaining side dot forms another singlet with an electron on the central dot. As a result, $G(T)$ is retained also at zero at low temperatures. Furthermore, in this regime, another singular two-stage Kondo effect is found, where the local spin on the central dot is screened by the electrodes firstly and then that on the remaining side dot (relative to those two side dots forming a spin singlet) is screened by the central spin through t_1, resulting in $\mu^2(T) \to 0$ as $T \to 0$. T_{K1} and T_{K2} are rather sensitive to the value of t_2. When t_2 is in the third quantum phase, the total charge number of subsystem $\mathbb{SD}$ drops to 2.0, and the side dots form a spin singlet due to t_2 and decouple from the central subsystem, resulting in the reappearance of the regular Kondo effect.

For fixed $t_1 \gg T_{K1}$, the partially recovered Kondo effect is demonstrated in the vicinity of $T \approx T_{K1}$, and the competition between J_{RKKY} and J_{DAE} is clearly revealed by the LDOS of the side dots.

When the energy level of the central dot sweeps downwards, one finds QPTs from an antiferromagnetic correlation among the side dots to a ferromagnetic one, and then to an antiferromagnetic one, accompanied by Kondo resonances in the LDOS of the central dot.

It is noted that for a bandwidth $W_b = 10^5$ K [75], the parameters in Figs. 3 and 7 give a maximum $T_{K2} \approx 10^{-1}$ K; hence our reported two-stage Kondo effects could be realized experimentally [76].

We believe that our present work not only clarifies the relevant strongly correlated physical picture of the singular two-stage Kondo behaviors and the quantum phase transition in the TQQD structure reported very recently, but also may provide important guidelines for experimental realization of nanoscale semiconductor tunneling devices and quantum computation hardware.

ACKNOWLEDGMENTS

We acknowledge sincerely the support from the NSFC under Grants No. 11504102 and No. 11904091, the Natural Science Foundation of Hubei Province under Grants No. 2019CFB788 and No. 2020CFB748, the Program for Science and Technology Innovation Team in Colleges of Hubei Province under Grant No. T2021012, the Hubei Key Laboratory of Automotive Power Train and Electronics [Hubei University of Automotive Technology (HUAT)] under Grant No. ZDK1202001, the Hubei Key Laboratory of Critical Materials of New Energy Vehicles (HUAT) under Grant No. QCCLSZK2021A05, and the Foundation of Discipline Innovation Team of HUAT.

[1] F. Jelezko, T. Gaebel, I. Popa, M. Domhan, A. Gruber, and J. Wrachtrup, Observation of Coherent Oscillation of a Single Nuclear Spin and Realization of a Two-Qubit Conditional Quantum Gate, Phys. Rev. Lett. **93**, 130501 (2004).

[2] L. Childress, M. V. G. Dutt, J. M. Taylor, A. S. Zibrov, F. Jelezko, J. Wrachtrup, P. R. Hemmer, and M. D. Lukin, Coherent dynamics of coupled electron and nuclear spin qubits in diamond, Science **314**, 281 (2006).

[3] J. J. Pla, K. Y. Tan, J. P. Dehollain, W. H. Lim, J. J. L. Morton, F. A. Zwanenburg, D. N. Jamieson, A. S. Dzurak, and A. Morello, High-fidelity readout and control of a nuclear spin qubit in silicon, Nature (London) **496**, 334 (2013).

[4] R. Prevedel, P. Walther, F. Tiefenbacher, P. Böhi, R. Kaltenbaek, T. Jennewein, and A. Zeilinger, High-speed linear optics quantum computing using active feed-forward, Nature (London) **445**, 65 (2007).

[5] I. Bloch, Quantum coherence and entanglement with ultracold atoms in optical lattices, Nature (London) **453**, 1016 (2008).

[6] V. M. Schäfer, C. J. Ballance, K. Thirumalai, L. J. Stephenson, T. G. Ballance, A. M. Steane, and D. M. Lucas, Fast quantum logic gates with trapped-ion qubit, Nature (London) **555**, 75 (2018).

[7] I. Chiorescu, Y. Nakamura, C. J. P. M. Harmans, and J. E. Mooij, Coherent quantum dynamics of a superconducting flux qubit, Science **299**, 1869 (2003).

[8] D. Q. Zhu, T. Jaako, Q. Y. He, and P. Rabl, Quantum Computing with Superconducting Circuits in the Picosecond Regime, Phys. Rev. Appl. **16**, 014024 (2021).

[9] M. N. Leuenberger and D. Loss, Quantum computing in molecular magnets, Nature (London) **410**, 789 (2001).

[10] A. Gaita-Ariño, F. Luis, S. Hill, and E. Coronado, Molecular spins for quantum computation, Nat. Chem. **11**, 301 (2019).

[11] I. L. Chuang, L. M. K. Vandersypen, X. Zhou, D. W. Leung, and S. Lloyd, Experimental realization of a quantum algorithm, Nature (London) **393**, 143 (1998).

[12] L. M. K. Vandersypen, M. Steffen, G. Breyta, C. S. Yannoni, M. H. Sherwood, and I. L. Chuang, Experimental realization of Shor's quantum factoring algorithm using nuclear magnetic resonance, Nature (London) **414**, 883 (2001).

[13] D. Loss and D. P. DiVincenzo, Quantum computation with quantum dots, Phys. Rev. A **57**, 120 (1998).

[14] K. C. Nowack, F. H. L. Koppens, Y. V. Nazarov and L. M. K. Vandersypen, Coherent control of a single electron spin with electric fields, Science **318**, 1430 (2007).

[15] A. Chatterjee, P. Stevenson, S. De Franceschi, A. Morello, N. P. de Leon, and F. Kuemmeth, Semiconductor qubits in practice, Nat. Rev. Phys. **3**, 157 (2021).

[16] A. Bogan, L. Bergeron, A. Kam, P. Zawadzki, S. Studenikin, L. Gaudreau, and A. Sachrajda, Strategies for tuning a linear quadruple quantum dot array to the few electron regime, Appl. Phys. Lett. **109**, 173108 (2016).

[17] D. P. DiVincenzo, Quantum computation, Science **270**, 255 (1995).

[18] S. Sasaki, S. De Franceschi, J. M. Elzerman, W. G. van der Wiel, M. Eto, S. Tarucha, and L. P. Kouwenhoven, Kondo effect in an integer-spin quantum dot, Nature (London) **405**, 764 (2000).

[19] R. M. Potok, I. G. Rau, H. Shtrikman, Y. Oreg, and D. Goldhaber-Gordon, Observation of the two-channel Kondo effect, Nature (London) **446**, 167 (2007).

[20] A. J. Keller, S. Amasha, I. Weymann, C. P. Moca, I. G. Rau, J. A. Katine, H. Shtrikman, G. Zaránd, and D. Goldhaber-Gordon, Emergent SU(4) Kondo physics in a spin-charge-entangled double quantum dot, Nat. Phys. **10**, 145 (2014).

[21] A. K. Mitchell and D. E. Logan, Two-channel Kondo phases and frustration-induced transitions in triple quantum dots, Phys. Rev. B **81**, 075126 (2010).

[22] Y. Tokura, H. Nakano, and T. Kubo, Interference through quantum dots, New J. Phys. **9**, 113 (2007).

[23] H. Zheng, S. Hou, C. Xin, Q. Wu, F. Jiang, Z. Tan, X. Zhou, L. Lin, W. He, Q. Li, J. Zheng, L. Zhang, J. Liu, Y. Yang, J. Shi, X. Zhang, Y. Zhao, Y. Li, C. Lambert, and W. Hong, Room-temperature quantum interference in single perovskite quantum dot junctions, Nat. Commun. **10**, 5458 (2019).

[24] R. A. Żak and K. Flensberg, Coulomb blockade of a three-terminal quantum dot, Phys. Rev. B **77**, 045329 (2008).

[25] M. Brotons-Gisbert, A. Branny, S. Kumar, R. Picard, R. Proux, M. Gray, K. S. Burch, K. Watanabe, T. Taniguchi, and B. D. Gerardot, Coulomb blockade in an atomically thin quantum dot coupled to a tunable Fermi reservoir, Nat. Nanotechnol. **14**, 442 (2019).

[26] H. Duprez, F. Pierre, E. Sivre, A. Aassime, F. D. Parmentier, A. Cavanna, A. Ouerghi, U. Gennser, I. Safi, C. Mora, and A. Anthore, Dynamical Coulomb blockade under a temperature bias, Phys. Rev. Research **3**, 023122 (2021).

[27] W. Hofstetter and H. Schoeller, Quantum Phase Transition in a Multilevel Dot, Phys. Rev. Lett. **88**, 016803 (2001).

[28] R. Žitko and J. Bonča, Quantum phase transitions in systems of parallel quantum dots, Phys. Rev. B **76**, 241305(R) (2007).

[29] A. K. Mitchell, T. F. Jarrold, and D. E. Logan, Quantum phase transition in quantum dot trimers, Phys. Rev. B **79**, 085124 (2009).

[30] W.-Z. Wang, Kondo effect and continuous quantum phase transitions in double quantum dots with on-site and interdot repulsion and magnetic field, Phys. Rev. B **83**, 075314 (2011).

[31] Q. Si and F. Steglich, Heavy fermions and quantum phase transitions, Science **329**, 1161 (2010).

[32] H. Lu, R. Lv, and B.-F. Zhu, Tunable Fano effect in parallel-coupled double quantum dot system, Phys. Rev. B **71**, 235320 (2005).

[33] R. Žitko, Fano-Kondo effect in side-coupled double quantum dots at finite temperatures and the importance of two-stage Kondo screening, Phys. Rev. B **81**, 115316 (2010).

[34] R. Žitko and J. Bonča, Fermi-Liquid versus Non-Fermi-Liquid Behavior in Triple Quantum Dots, Phys. Rev. Lett. **98**, 047203 (2007).

[35] X. Wang and A. J. Millis, Quantum criticality and non-Fermi-liquid behavior in a two-level two-lead quantum dot, Phys. Rev. B **81**, 045106 (2010).

[36] D. E. Logan, A. P. Tucker, and M. R. Galpin, Common non-Fermi liquid phases in quantum impurity physics, Phys. Rev. B **90**, 075150 (2014).

[37] Z.-T. Jiang and Q.-Z. Han, Quantum coherent transport through a quadruple quantum-dot structure with one continuous channel and two concrete channels, Phys. Rev. B **78**, 035307 (2008).

[38] D. E. Liu, S. Chandrasekharan, and H. U. Baranger, Quantum Phase Transition and Emergent Symmetry in a Quadruple Quantum Dot System, Phys. Rev. Lett. **105**, 256801 (2010).

[39] B. Sothmann, J. Li, and M. Büttiker, Fractional Josephson effect in a quadruple quantum dot, New J. Phys. **15**, 085018 (2013).

[40] R. Shang, H.-O. Li, G. Cao, G. Yu, M. Xiao, T. Tu, G.-C. Guo, H. Jiang, A. M. Chang, and G.-P. Guo, Observation of the Kondo effect in a quadruple quantum dot, Phys. Rev. B **91**, 245102 (2015).

[41] M. Y. Kagan, V. V. Val'kov, and S. V. Aksenov, Coulomb interactions-induced perfect spin-filtering effect in a quadruple quantum-dot cell, J. Magn. Magn. Mater. **440**, 15 (2017).

[42] V. S. Protsenko and A. A. Katanin, Local magnetic moments and electronic transport in closed loop quantum dot systems: A case of quadruple quantum dot ring at and away from equilibrium, Phys. Rev. B **99**, 165114 (2019).

[43] J. Choi, G. Yoo, C. Han, and H.-S. Sim, Charge Kondo effects in a quadruple quantum dot in spinless and spinful regimes, Phys. Rev. B **101**, 245307 (2020).

[44] T. Takakura, A. Noiri, T. Obata, T. Otsuka, J. Yoneda, K. Yoshida, and S. Tarucha, Single to quadruple quantum dots with tunable tunnel couplings, Appl. Phys. Lett. **104**, 113109 (2014).

[45] M. R. Delbecq, T. Nakajima, T. Otsuka, S. Amaha, J. D. Watson, M. J. Manfra, and S. Tarucha, Full control of quadruple quantum dot circuit charge states in the single electron regime, Appl. Phys. Lett. **104**, 183111 (2014).

[46] A. C. Betz, M. L. V. Tagliaferri, M. Vinet, M. Broström, M. Sanquer, A. J. Ferguson, and M. F. Gonzalez-Zalba, Reconfigurable quadruple quantum dots in a silicon nanowire transistor, Appl. Phys. Lett. **108**, 203108 (2016).

[47] J. Mu, S. Huang, Z.-H. Liu, W. Li, J.-Y. Wang, D. Pan, G.-Y. Huang, Y. Chen, J. Zhao, and H. Q. Xu, A highly tunable quadruple quantum dot in a narrow bandgap semiconductor InAs nanowire, Nanoscale **13**, 3983 (2021).

[48] T. Ito, T. Otsuka, T. Nakajima, M. R. Delbecq, S. Amaha, J. Yoneda, K. Takeda, A. Noiri, G. Allison, A. Ludwig, A. D. Wieck, and S. Tarucha, Four single-spin Rabi oscillations in a quadruple quantum dot, Appl. Phys. Lett. **113**, 093102 (2018).

[49] A. J. Sigillito, J. C. Loy, D. M. Zajac, M. J. Gullans, L. F. Edge, and J. R. Petta, Site-Selective Quantum Control in an Isotopically Enriched $^{28}Si/Si_{0.7}Ge_{0.3}$ Quadruple Quantum Dot, Phys. Rev. Appl. **11**, 061006(R) (2019).

[50] R. Thalineau, S. Hermelin, A. D. Wieck, C. Bäuerle, L. Saminadayar, and T. Meunier, A few-electron quadruple quantum dot in a closed loop, Appl. Phys. Lett. **101**, 103102 (2012).

[51] S. F. Neyens, E. R. MacQuarrie, J. P. Dodson, J. Corrigan, N. Holman, B. Thorgrimsson, M. Palma, T. McJunkin, L. F. Edge, M. Friesen, S. N. Coppersmith, and M. A. Eriksson,

Measurements of Capacitive Coupling within a Quadruple-Quantum-Dot Array, Phys. Rev. Appl. **12**, 064049 (2019).

[52] J. Leemans, K. C. Dümbgen, M. M. Minjauw, Q. Zhao, A. Vantomme, I. Infante, C. Detavernier, and Z. Hens, Acid-base mediated ligand exchange on near-infrared absorbing, indium-based III–V colloidal quantum dots, J. Am. Chem. Soc. **143**, 4290 (2021).

[53] S. Id Bakas and M. El Hafidi, Frustration effect and possibility of spin quantum liquid state in a tetrahedral spin 1/2 molecule, Chin. J. Phys. **73**, 433 (2021).

[54] P. Földi, O. Kálmán, M. G. Benedict, and F. M. Peeters, Networks of quantum nanorings: Programmable spintronic devices, Nano Lett. **8**, 2556 (2008).

[55] H.-H. Fu and K.-L. Yao, Perfect spin-filter and highly spin-polarized current in a quantum network device, Appl. Phys. Lett. **100**, 013502 (2012).

[56] L. H. G. Kalinke, D. Cangussu, M. Mon, R. Bruno, E. Tiburcio, F. Lloret, D. Armentano, E. Pardo, and J. Ferrando-Soria, Metal-organic frameworks as playgrounds for reticulate single-molecule magnets, Inorg. Chem. **58**, 14498 (2019).

[57] H. R. Krishna-murthy, J. W. Wilkins, and K. G. Wilson, Renormalization-group approach to the Anderson model of dilute magnetic alloys. I. Static properties for the symmetric case, Phys. Rev. B **21**, 1003 (1980).

[58] R. Bulla, T. A. Costi, and T. Pruschke, Numerical renormalization group method for quantum impurity systems, Rev. Mod. Phys. **80**, 395 (2008).

[59] R. Žitko and T. Pruschke, Energy resolution and discretization artifacts in the numerical renormalization group, Phys. Rev. B **79**, 085106 (2009).

[60] J. R. Schrieffer and P. A. Wolff, Relation between Anderson and Kondo Hamiltonians, Phys. Rev. **149**, 491 (1966).

[61] E. Lieb and D. Mattis, Ordering energy levels of interacting spin systems, J. Math. Phys. (Melville, NY) **3**, 749 (1962).

[62] R. Landauer, Spatial variation of currents and fields due to localized scatterers in metallic conduction, IBM J. Res. Dev. **1**, 223 (1957).

[63] Y. Meir, N. S. Wingreen, and P. A. Lee, Low-Temperature Transport through a Quantum Dot: The Anderson Model Out of Equilibrium, Phys. Rev. Lett. **70**, 2601 (1993).

[64] A. Weichselbaum and J. von Delft, Sum-Rule Conserving Spectral Functions from the Numerical Renormalization Group, Phys. Rev. Lett. **99**, 076402 (2007).

[65] I. Weymann, Finite-temperature spintronic transport through Kondo quantum dots: Numerical renormalization group study, Phys. Rev. B **83**, 113306 (2011).

[66] F. D. M. Haldane, Theory of the atomic limit of the Anderson model. I. Perturbation expansions re-examined, J. Phys. C: Solid State Phys. **11**, 5015 (1978).

[67] P. S. Cornaglia and D. R. Grempel, Strongly correlated regimes in a double quantum dot device, Phys. Rev. B **71**, 075305 (2005).

[68] A. E. Miroshnichenko, S. Flach, and Y. S. Kivshar, Fano resonances in nanoscale structures, Rev. Mod. Phys. **82**, 2257 (2010).

[69] W.-Z. Wang, Spectral properties and quantum phase transitions in parallel triple quantum dots, Phys. Rev. B **76**, 115114 (2007).

[70] Y. C. Xiong, W. Z. Wang, S. J. Luo, J. T. Yang, and H. M. Huang, RKKY interaction and local density of states for a triangular triple quantum dot system, J. Magn. Magn. Mater. **399**, 5 (2016).

[71] R. Žitko and J. Bonča, Multiple-impurity Anderson model for quantum dots coupled in parallel, Phys. Rev. B **74**, 045312 (2006).

[72] J. A. Andrade, D. J. García, and P. S. Cornaglia, Ferromagnetic and underscreened Kondo behavior in quantum dot arrays, Phys. Rev. B **92**, 165416 (2015).

[73] G. Chiappe, E. V. Anda, L. C. Ribeiro, and E. Louis, Kondo regimes in a three-dots quantum gate, Phys. Rev. B **81**, 041310(R) (2010).

[74] T. A. Costi, A. C. Hewson, and V. Zlatić, Transport coefficients of the Anderson model via the numerical renormalization group, J. Phys.: Condens. Matter **6**, 2519 (1994).

[75] A. A. Aligia, Effective Kondo Model for a Trimer on a Metallic Surface, Phys. Rev. Lett. **96**, 096804 (2006).

[76] X. Guo, Q.-H. Zhu, L.-Y. Zhou, W. Yu, W.-G. Lu, and W.-J. Liang, Evolution and universality of two-stage Kondo effect in single manganese phthalocyanine molecule transistors, Nat. Commun. **12**, 1566 (2021).